EDGE ARTICLE

Bright and sensitive ratiometric fluorescent probe enabling endogenous FA imaging and mechanistic exploration of indirect oxidative damage due to FA in various living systems†

Kun Dou,[a] Guang Chen, [ID] *[abc] Fabiao Yu,[b] Yuxia Liu,[a] Lingxin Chen, [ID] [b] Ziping Cao,[a] Tao Chen,[c] Yulin Li[c] and Jinmao You*[ab]

As a notorious toxin, formaldehyde (FA) poses an immense threat to human health. Aberrantly elevated FA levels lead to serious pathologies, including organ damage, neurodegeneration, and cancer. Unfortunately, current techniques limit FA imaging to general comparative studies, instead of a mechanistic exploration of its biological role, and this is presumably due to the lack of robust molecular tools for reporting FA in living systems. More importantly, despite being reductive, FA, however, can induce oxidative damage to organisms, thus providing a challenge to the mechanistic study of FA using fluorescence imaging. Herein, we presented the design and multi-application of a bright sensitive ratiometric fluorescent probe 1-(4-(1*H*-phenanthro[9,10-*d*]imidazol-2-yl)phenyl) but-3-en-1-amine (**PIPBA**). With a π-extended phenylphenanthroimidazole fluorophore and an allylamine group, **PIPBA** exhibited high quantum yield ($\phi = 0.62$) in blue fluorescent emission and selective reactivity toward FA. When sensing FA, **PIPBA** transformed to PIBE, which is a product capable of releasing bright green fluorescence ($\phi = 0.51$) with its enhanced intramolecular charge transfer (ICT). Transformation of **PIPBA** to PIBE contributed to 80 nm of red shift in emission wavelength and a highly sensitive ratiometric response (92.2-fold), as well as a quite low detection limit (0.84 μM). **PIPBA** was successfully applied to various living systems, realizing, for the first time, ratiometric quantification (in cells), *in vivo* imaging (zebrafish), and living tissue imaging (vivisectional mouse under anaesthetic) of endogenous FA that was spontaneously generated by biological systems. Furthermore, with the aid of **PIPBA**, we obtained visual evidence for the oxidative damage of FA in both HeLa cells and renal tissue of a living mouse. The results demonstrated that FA exerted indirect oxidative damage by interacting with free radicals, thus producing more oxidizing species, which eventually caused aggravated oxidative damage to the organism. The indirect oxidative damage due to FA could be alleviated by an exogenous or endogenous antioxidant. The excellent behaviors of **PIPBA** demonstrate that a chemical probe can detect endogenous FA in cells/tissue/*vivo*, promising to be an effective tool for further exploration of the biological mechanism of FA in living systems.

Introduction

Formaldehyde (FA) has been extensively utilized in various fields including the chemical industry,[1] medical science,[2]

[a]The Key Laboratory of Life-Organic Analysis, Key Laboratory of Pharmaceutical Intermediates and Analysis of Natural Medicine, College of Chemistry and Chemical Engineering, Qufu Normal University, Qufu 273165, China. E-mail: chenandguang@163.com; jmyou6304@163.com

[b]Key Laboratory of Coastal Environmental Processes and Ecological Remediation, Yantai Institute of Coastal Zone Research, Chinese Academy of Sciences, Yantai 264003, China

[c]Key Laboratory of Tibetan Medicine Research, Qinghai Key Laboratory of Qinghai-Tibet Plateau Biological Resources, Northwest Institute of Plateau Biology, Chinese Academy of Science, Xining 810001, Qinghai, PR China

† Electronic supplementary information (ESI) available. See DOI: 10.1039/c7sc03719h

biotechnology,[3,4] *etc.* In living systems, FA plays a vital role in carbon cycle metabolism. FA can be generated by organisms *via* many processes, including as an intermediate in methylotrophic metabolism, from the degradation of glycine or heme, as the product of histones demethylation or methylated-DNA repair, or by the action of *N*-methyltryptophan oxidase.[5–8] Unfortunately, as a notorious toxin and carcinogen, FA poses an immense threat to human health.[9] On the macro level, FA exposure is carcinogenic and has a detrimental influence on the growth and reproductive development of organisms.[5,10] FA causes damage to the urinary system, inducing tubular degeneration and enlargement of peritubular vessels, as well as the dilatation in the distal tubules of kidneys.[11] On the cellular level, FA exerts protein toxicity by modifying the functional components in vital cells, thereby leading to cellular dysfunction.[12,13]

On the molecular level, FA can react with free thiol and amine groups on protein or DNA, which is followed by the formation of irreversible FA-adducts,[14] as well as FA-catalyzed cross-links of DNA and/or proteins.[15] Nevertheless, there are many issues about the toxicity mechanism of FA that need to be addressed. For example, from the perspective of its chemical properties, FA should be a strong reductant, however, it causes oxidative damage to organisms.[16,17] Unfortunately, up to now, the biological roles of FA in terms of its oxidative toxicity mechanism have not been well-defined. Furthermore, in the presence of reactive oxygen species (ROS), FA causes aggravated damage to organisms,[18] which provides a challenge for further exploration of FA in living systems.

Therefore, it is imperative to study in detail FA in living cells, in tissue, and *in vivo*, in order to to reveal its oxidative toxicity mechanism. For this study, the main difficulty lies in the fact that it is almost impossible to separate FA immediately from living systems, and thus conventional methods, such as gas chromatography[19] and high performance liquid chromatography,[20] cannot meet the requirements. Fluorescence imaging has become an efficient means to track analytes in living systems owing to its excellent spatiotemporal resolution and non-invasive properties.[21–27] Many desirable fluorescent probes for reporting FA in living systems have been designed, most of which are available for FA imaging in cells[21,28–31] and few can be applied in living tissue.[32,33] To the best of our knowledge, imaging of endogenous FA *in vivo* has not yet been realized, which limits the study of FA in various living biological samples. Furthermore, current probes are mainly used for qualitative comparative studies, and lack the quantitative measurements and in-depth study of FA with regard to its biological role.

To improve the status for FA study, we consider the issues in designing a robust molecular tool for probing endogenous FA in living organisms. First, the level of endogenous FA that is spontaneously generated by an organism is low. Thus, we need a probe capable of exhibiting a highly sensitive response to trace amounts of FA in living systems. Second, imaging assays *in vivo* or in living tissue need a strong fluorescence signal that can penetrate the thick tissue of living systems. In such a case, a bright fluorescent probe with a high quantum yield is much needed. Especially in an intravital experiment on mammal, like a mouse, the intravenous or intraperitoneal injection of a bright probe may allow the clear imaging of FA in living tissue or *in vivo*. Third, another challenge lies in the accuracy of imaging analysis for FA in living systems. Practically, there are too many disturbing factors in biological systems, including a varying microenvironment, heterogeneous distribution of the analyte, and the uneven localization of probe. Thus, in order to solve the above issues, this sensitive and bright probe should preferably possess a ratiometric response toward the target. Moreover, the synergetic fluorescence responses of a ratiometric probe may contribute to improving quantitative reliability and avoiding spectral overlap and photobleaching.[34] Consequently, we need a bright, sensitive ratiometric fluorescent probe that can selectively track FA in various living systems, which unfortunately cannot be found by us despite the notable progress in FA

imaging contributed by pioneering scientists in recent years.[21,28–32,35–40]
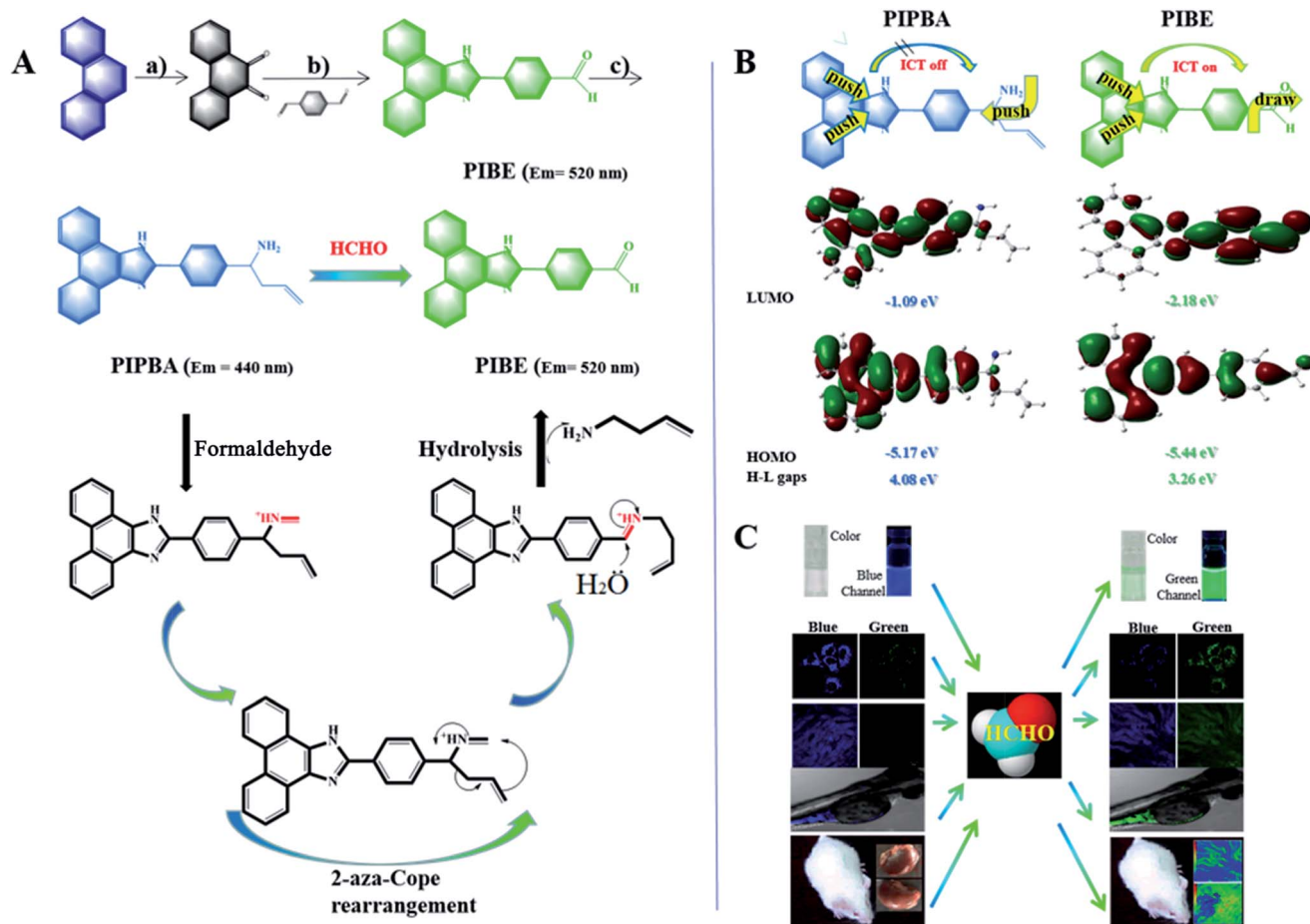
In this work, we designed a new bright and sensitive ratiometric fluorescent probe 1-(4-(1*H*-phenanthro[9,10-*d*]imidazol-2-yl)phenyl) but-3-en-1-amine (**PIPBA**) for imaging endogenous FA in cells, zebrafish, and the renal tissue of a living mouse. To seek a high fluorescence intensity and good photostability, we chose phenanthrene as the starting material and modified it to a π-extended fluorophore, PIBE, which could release strong green fluorescence *via* an enhanced intramolecular charge transfer (ICT) (Scheme 1). To achieve a sensitive response, we modified PIBE with an allylamine group, obtaining the probe **PIPBA**, which exhibited bright blue fluorescence with the shrunken π-conjugation. Furthermore, the allylamine group of **PIPBA** acted as the electron donor, thus leading to a restricted ICT (ICT off). **PIPBA** could selectively react with FA *via* first the imine ions formation, then 2-aza-Cope rearrangement, and finally hydrolysis, producing PIBE. When sensing FA, transformation of **PIPBA** to the product PIBE contributed to the 80 nm of red shift in emission wavelength and the significantly increased fluorescence ratio (92.2-fold). The sensitive ratio response endowed **PIPBA** with a fairly low detection limit (0.84 μM) toward FA. With the satisfactory properties of **PIPBA** in mind, we performed series of studies using confocal imaging to explore, in-depth, FA in various biological samples. First, the imaging and quantification of intracellular endogenous FA were realized. Second, the mechanism of indirect oxidative damage from intracellular FA in the presence of a radical initiator was visually explored. Third, the *in vivo* imaging of endogenous FA in zebrafish was achieved. Fourth, **PIPBA** was injected intraperitoneally into a mouse, enabling the imaging of endogenous FA in the renal tissue of the living mouse under anaesthetic. The indirect oxidative damage due to FA was verified in the kidney of the living mouse. The alleviating effects of endogenous and exogenous anti-oxidants on the oxidative damage due to FA to renal tissue were explored.

Results and discussion

Design strategy of probe PIPBA

We previously applied phenanthrene to the design of a fluorescent reagent for derivatisation, and found that this fluorophore possessed a high fluorescence intensity with good photostability.[41–43] At the beginning of this design, we found that, when phenanthrene was equipped with two carbonyls, this molecule became phenanthraquinone and its violet fluorescence was remarkably quenched (Scheme 1A). These phenomena indicated that phenanthrene could be modified to enable the regulation of molecular fluorescence, which inspired us to engineer a bright fluorescent probe enjoying controllable intramolecular charge transfer (ICT). Then, we integrated 1,4-phthalaldehyde with phenanthraquinone, achieving the fluorescent molecule PIBE. Compared to phenanthraquinone, PIBE had a larger π-conjugated structure. Moreover, the oxygen in its aldehyde group could serve as a strong electron acceptor, and thus might enable the effective ICT (Scheme 1B). Next, for the selective reporting of FA, we equipped an allylamine group to

Scheme 1 (A) The design strategy for probe **PIPBA** and the proposed sensing mechanism of **PIPBA** for formaldehyde. (a) NaClO, tetrabuty-lammonium hydrogen sulfate; (b) ammonium acetate, acetic acid, reflux, 30 min; (c) NH$_3$ in CH$_3$OH, allylboronic acid pinacol ester, temperature, overnight. (B) Frontier molecular orbital plots and electron transfer sketches for probe **PIPBA** and product PIBE. The green and red shapes correspond to different phases of the molecular wave functions for the HOMO and LUMO orbitals. (C) The promising application of probe **PIPBA** in cells, zebrafish, and kidney tissue on the basis of the design of the probe.

PIBE. The resultant Schiff base underwent a nucleophilic addition with allylboronic acid pinacol ester, forming the probe **PIPBA** (Scheme 1A; Fig. S1†). Our experiences let us expect that such design may endow many attractive properties to probe **PIPBA**.[25,44–46] First, the allylamine group in **PIPBA** will react selectively with FA, initially undergoing imine formation, then the 2-aza-Cope rearrangement and finally hydrolysis, with PIBE obtained as the product (Scheme 1A). Such a reaction mechanism should be suitable for the detection of FA at low concentrations.[29,47] Second, unlike the amino group in **PIPBA**, the aldehyde oxygen in PIBE would act as not an electron donor but as an electron acceptor. Thus the product PIBE should exhibit completely different electron push–pull comparing with **PIPBA**, which is beneficial for an intense fluorescence response toward FA. Third, product PIBE had larger distribution of π-electronic conjugations than probe **PIPBA**. Thus, a red shift in fluorescence emission could be expected when probe **PIPBA** responded to FA, which might contribute to the ratiometric detection. Fourth, with the high quantum yield and the sensitive fluorescence response, there was the potential that probe **PIPBA** could

be used in various biological systems such as in cells, in living tissue, and *in vivo*. To confirm this design, we carried out a series of verifying experiments. Firstly, the reaction of **PIPBA** with FA was performed and monitored on-line using HPLC-UV. From Fig. S2-B,† we found that two peaks appeared separately. To identify the two compounds, we prepared pure **PIPBA** (Fig. S2-A†) and PIBE (Fig. S2-C†). As can be seen, there was a good overlap for these corresponding peaks, indicating that the product of this reaction should be PIBE. Secondly, to get further identification, MS was applied to monitor the reaction of **PIPBA** with FA. As shown in Fig. S3,† a peak at *m/z* 322.8 was observed, demonstrating that the product was PIBE. Thirdly, the product was separated from the reaction of **PIPBA** with FA, and was purified using silica column chromatography. This product was characterized using ^{1}H NMR, ^{13}C NMR, and MS (Fig. S4†). The results justified the interpretation that the structural information of this product belonged to PIBE. Fourthly, the comparison of ^{1}H NMR between the synthetic PIBE and the isolated product from the reaction of **PIPBA** with FA was made. The results shown in Fig. S5† indicated that the

product was PIBE, as we designed. Therefore, the probe **PIPBA** proven to be able to react with FA following the design.

Optical response and sensing mechanism of PIPBA toward FA

Optical response and sensing mechanism of **PIPBA** toward FA were investigated. As seen from UV spectra (Fig. 1A), with the addition of FA, absorption peak at 310 nm declined and a new peak at 380 nm rose up, which was corresponding respectively to the exhaustion of probe **PIPBA** and the formation of product PIBE. As shown in Fig. 1B, probe **PIPBA** (5 μM) itself exhibited fluorescence emission at 440 nm ($\phi = 0.62$). Upon addition of FA, the emission peak at 440 nm decreased and a new emission at 520 nm ($\phi = 0.51$) arose, exhibiting a synergetic response to the increased FA level. Clearly, compared to probe **PIPBA**, product PIBE displayed 80 nm of red shift in fluorescence emission with a well-defined isosbestic point at 500 nm. In order to understand the sensing mechanism, we dissected the molecular orbitals, HOMO (highest occupied molecular orbital) and LUMO (lowest unoccupied molecular orbital) of PIBE and **PIPBA**, using density functional theory (DFT).[48–51] As shown in Scheme 1B, probe **PIPBA** exhibited a smaller π-distribution than product PIBE, because the saturated carbon in the allyl-amine group broke the π-conjugation in **PIPBA**. In PIBE, the aldehyde oxygen (electron-withdrawing) participated in the π-conjugation and extended the π-distribution, and this was responsible for the fluorescence red shift. Moreover, the estimation of orbital energy indicated that the energy gap between the HOMO and LUMO was smaller in product PIBE than in probe **PIPBA**. Thus, PIBE could release a lower energy than **PIPBA**, which further accounted for the fluorescence red shift. Therefore, probe **PIPBA** proved to be able to display the desired optical properties for sensing FA. With these satisfactory properties, we then tested the capability of **PIPBA** to quantify FA.[52] First, we investigated the dynamic fluorescence response of **PIPBA** to FA at two emission wavelengths (440 nm; 520 nm). Fig. S6† provided the synergetic information for **PIPBA** exhaustion and PIBE production during the reaction. Also, this result showed that within 30 min linear responses at the two respective wavelengths could be achieved. Second, we tested the time-dependent ratiometric responses ($I_{520\ nm}/I_{440\ nm}$). Fig. 1C shows the kinetic curves, with which the corresponding pseudo-first order rate constants were calculated to be 0.028 min^{-1} (200 μM) and 0.078 min^{-1} (500 μM), respectively. Comparing the above results, we found that, though the linear ratiometric response could be obtained in 30 min, it needed about 60–80 min for the ratiometric response to reach the maximum and stable value. Therefore, the following experiments were performed with the reaction time of 2 h to obtain the stable signals. Third, the linear trend for ratiometric quantification ($I_{520\ nm}/I_{440\ nm}$) of FA was established. As shown in Fig. 1D, a dose-dependent ratiometric linearity ($R^2 = 0.9949$) for FA (0–0.6 mM) was achieved. Thus **PIPBA** should be able to quantify FA in a wide concentration range. Fourth, to evaluate the capacity of **PIPBA** for tracking low levels of FA, we calculated the detection limit (ESI†). The result showed that **PIPBA** provided a fairly low detection limit of 0.84 μM, which is comparable to those of the most sensitive probes for FA.[33] These excellent properties demonstrated that **PIPBA** could provide a strong and sensitive response for the ratiometric quantification of FA.
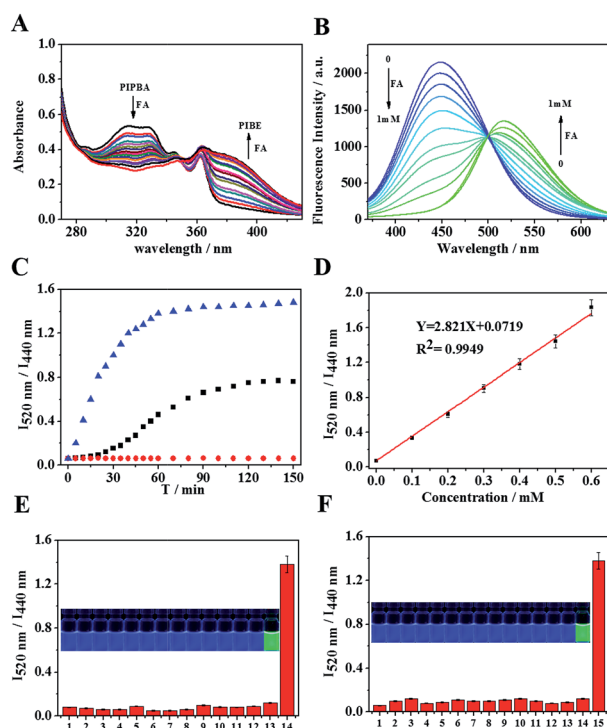

Fig. 1 (A) UV-vis of probe **PIPBA** (5 μM) upon addition of formaldehyde (0 to 1 mM). (B) Fluorescence response of probe **PIPBA** (5 μM) to formaldehyde (0 to 1 mM) ($\lambda_{ex} = 350$ nm). (C) Time-dependent fluorescence ratios of the probe **PIPBA** (5 μM) in the absence [●] or presence of formaldehyde (200 μM [■] and 500 μM [▲]). (D) The linear curve established using the fluorescence ratios ($I_{520\ nm}/I_{440\ nm}$) versus the concentrations of FA (0 to 0.6 mM). (E) The selectivity tests for probe **PIPBA** (5 μM) in the presence of various compounds (0.5 mM) (1: glyoxal, 2: acetaldehyde, 3: methylglyoxal, 4: 4-methoxybenzaldehyde, 5: 4-nitrobenzaldehyde, 6: acetone, 7: benzaldehyde, 8: GSH, 9: Cys, 10: Hcy, 11: H_2O_2, 12: ClO^-, 13: HS^-, 14: HSO_3^-, and 15: formaldehyde), with the fluorescence intensity ratio ($I_{520\ nm}/I_{440\ nm}$) as the scale plate. (F) The selectivity tests for probe **PIPBA** (5 μM) against various metal ions (0.5 mM): 1: Fe^{3+}, 2: Co^{2+}, 3: Ni^{2+}, 4: Zn^{2+}, 5: Hg^{2+}, 6: Mn^{2+}, 7: Ag^+, 8: Cd^{2+}, 9: Na^+, 10: K^+, 11: Mg^{2+}, 12: Al^{3+}, 13: Cu^{2+}, 14: formaldehyde. Inset: the change of fluorescence color in the dark. All experiments were conducted in DMSO/PBS buffer solution (50/50, v/v, pH = 7.4, 20 mM).

Selectivity test

Before application, the selectivity of this probe to FA against possible interferences was tested. Considering the reactive nature of the aldehyde functionality, we investigated whether biologically relevant aldehyde species could provide interference using glyoxal, acetaldehyde, methylglyoxal, 4-methoxybenzaldehyde, 4-nitrobenzaldehyde, and acetone (Fig. 1E). Moreover, considering that **PIPBA** contains an allyl group that might react with nucleophilic and oxidative reagents, the reactive sulfur species HS^- HSO_3^-, GSH, Cys, and Hcy, as well as representative oxygen species (H_2O_2, HClO) were considered in the selectivity experiments. Additionally, conventional metal

ions were also evaluated in this test. As shown in Fig. 1E and F, these substances caused negligible interference. Therefore, the developed probe could selectively report FA without interference from biologically relevant analytes.

Imaging endogenous FA that is spontaneously generated in living cells

The above properties promoted us to explore the imaging of FA in living cells. Before cell imaging, the cytotoxicity of **PIPBA** to living cells was evaluated using MTT assay. When living HeLa cells were pre-treated with various concentrations of probe (0–25 μM) for 24 h, there were no significant changes to the cells' viability (more than 90% of cells were alive) (Fig. S9†), suggesting that **PIPBA** has low toxicity to living cells. Then, we investigated the penetration and photostability of **PIPBA** in cells (Fig. S10†). The results indicated that **PIPBA** could penetrate into the cells and release a stable fluorescence signal in 40 min, which helped us to design the following experiments. Based on these results, we began to perform the fluorescence detection of intracellular FA using probe **PIPBA**. In view of different experimental difficulties, we carried out these experiments with four stages, step by step. In the first stage, we verified the capability of **PIPBA** to report intracellular FA using its syngeneic fluorescence responses in two channels. Living HeLa cells were pre-treated with 5 μM of **PIPBA** for 0.5 h in culture medium. As can be seen in Fig. 2A-a, without the addition of exogenous FA, the cells exhibited fluorescence in the green channel upon the addition of probe **PIPBA**. This green fluorescence was probably caused by endogenous FA, which was validated in detail by us in the second stage of intracellular experiments. In such a case, we added various levels of FA (0 μM −1000 μM) to the **PIPBA**-treated cells to verify that fluorescence responses of the two channels were induced by FA. As shown in Fig. 2A-b–e, the cells responded to the increased FA with weakened fluorescence intensity in the blue channel and enhanced fluorescence intensity in the green channel. Clearly, these synergetic responses indicated the exhaustion of probe **PIPBA** and the production of PIBE inside the cells. Therefore, the fluorescence signals collected from the two channels could report intracellular FA. To preclude the potential auto-fluorescence of biological samples, a series of control experiments were carried out (Fig. S12†). The results showed that the cell (as well as other samples) itself displayed essentially no emission in both the blue and green channels, whereas the **PIPBA**-treated samples exhibited synergetic fluorescence in the two channels. These results indicated that under this experimental condition, the confocal imaging assay would not suffer from the interference of auto-fluorescence from the tested biological samples. Then, to further confirm that the fluorescence responses were induced by FA, a flow cytometry assay was performed, since flow cytometry techniques could provide rapid quantification of large cell populations. As shown in Fig. 2B, there were clear peak shifts toward the high intensity, in response to an elevated amount of FA. These shifts were consistent with the enhanced fluorescence intensity that was recorded using confocal fluorescence microscopy. Therefore, the above experiments
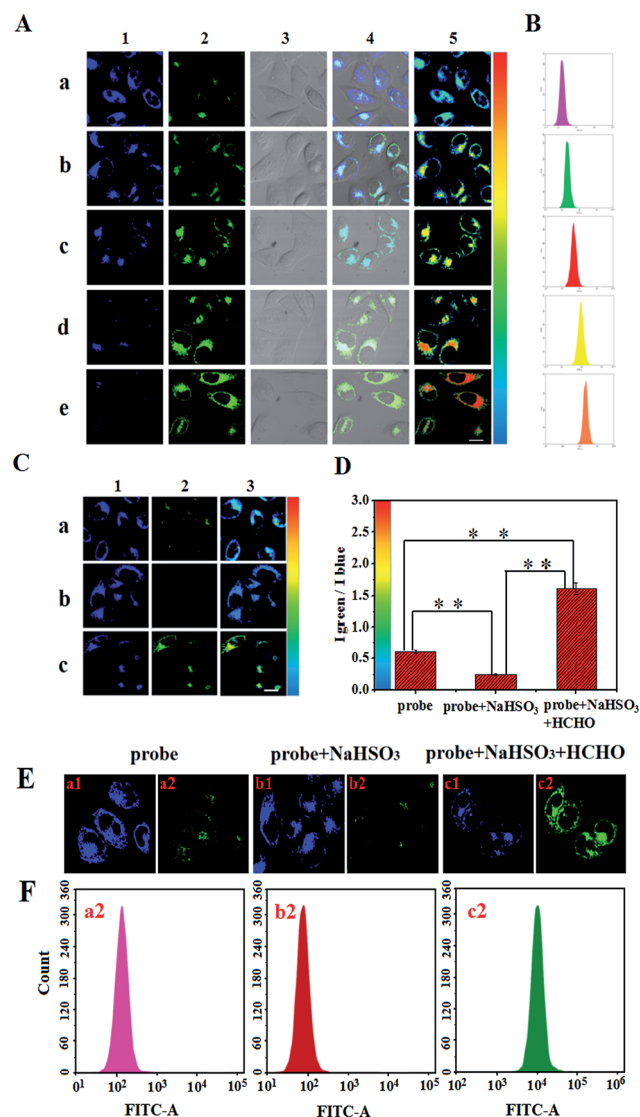

Fig. 2 Confocal fluorescence images for monitoring intracellular formaldehyde. (A) HeLa cells were incubated first with **PIPBA** (5 μM), then with different levels of formaldehyde ((a) 0 μM, (b) 150 μM, (c) 400 μM, (d) 750 μM, and (e) 1 mM) for 2 h. (B) Flow cytometry assays were performed to further validate the results from confocal imaging (ex = 488 nm). Collected wavelengths were 500–560 nm (fluorescein isothiocyanate FITC). (C) Confocal fluorescence images for endogenous formaldehyde. (a) HeLa cells were incubated with **PIPBA** (5 μM) for 2 h, (b) cells were pre-treated with 200 μM HSO_3^- for 30 min and then with **PIPBA** (5 μM) for 2 h, where HSO_3^- was a scavenger to consume endogenous formaldehyde), and (c) the cells of group b were incubated with exogenous 500 μM of formaldehyde for 2 h. (D) The average fluorescence intensity ratios of I_{green}/I_{blue} ((C) (a/b/c)) were calculated, and statistical analysis was performed using the Students t-test ($n = 10$ fields of cells), **$P < 0.01$. (E and F) Confocal imaging and flow cytometry assay for endogenous formaldehyde (ex = 488 nm and collected wavelengths were 500–560 nm (FITC). Green channel ($\lambda_{ex} = 405$ nm, $\lambda_{em} = 480$–580 nm), blue channel ($\lambda_{ex} = 405$ nm, $\lambda_{em} = 420$–480 nm), ratio imaging (I_{green}/I_{blue}). Scale bar: 20 μm.

demonstrated that probe **PIPBA** could report intracellular FA with its synergetic fluorescence responses in two channels using confocal imaging.

For the second stage, we investigated the ability of **PIPBA** to detect the endogenous FA that was spontaneously generated in living cells. As shown in Fig. 2C-a, when probe **PIPBA** (5 μM) was added to intact HeLa cells, strong fluorescence in the blue channel and weak fluorescence in the green channel were observed, which was consistent with the phenomena shown in Fig. 2A-a. These phenomena suggested that, without exogenous addition and stimulation to cells, the collected fluorescence responses or fluorescence ratios should be induced by the endogenous FA. In order to demonstrate this point, a FA scavenger,[33] HSO_3^-, was selected for the following verification experiments, because it could serve as a strong nucleophile for the rapid and complete removal of FA after penetration into the cells. We pre-treated the intact HeLa cells with HSO_3^- (200 μM) for 30 min, and then with **PIPBA** (5 μM) for another 2 h. We expected that HSO_3^- could react with endogenous FA to destroy its central carbonyl structure, and thus the endogenous FA could be removed. As shown in Fig. 2C-b, the fluorescence intensity in the green channel was dramatically weakened and the bright fluorescence in the blue channel was collected, in contrast to Fig. 2C-a. These results should be attributed to the scavenging effect of HSO_3^- on the intracellular FA, which in turn demonstrated that the fluorescence in the green channel (Fig. 2C-a) was induced by intracellular spontaneously generated FA. For the further confirmation of this point, we added exogenous FA (500 μM) to the cells that were pretreated with HSO_3^-. From the results shown in Fig. 2C-c, we observed obvious bright green fluorescence and weakened blue fluorescence. Clearly, these phenomena were caused by the addition of increasing amount of FA, which in turn confirmed the spontaneously generated FA that was detected in Fig. 2C-a. Finally, to further validate above results, we analyzed the cells using flow cytometry. As shown in Fig. 2F-a2 and b2, the green fluorescence shifted toward the low intensity area in the FITC channel of the flow cytometry after the HSO_3^- was added to the cells of group a. When the exogenous FA was added to the cells of group b, the peak shifted toward the high intensity area in the FITC channel of the flow cytometry. Thus, the flow cytometry assay further confirmed that the fluorescence response of **PIPBA** was induced by the intracellular spontaneous FA. Therefore, it could be concluded that **PIPBA** was able to report the spontaneously generated FA in HeLa cells.

In the third stage, based on the above investigations, we tried to achieve the relative quantification of FA in cells. Using probe **PIPBA**, we collected the fluorescence intensity from the two channels and calculated the ratios, I_{green}/I_{blue}, as illustrated in Fig. 2C-3 and D. According to the calibration in Fig. 1d, the average concentrations of FA in intact cells were estimated to be 156 μM (SD = ±0.27, $n = 11$). In contrast, upon the pretreatment with HSO_3^- (200 μM) for 30 min, cells showed around 61 μM (SD = ±0.14, $n = 11$) FA. After the addition of extra FA, the concentration of FA rose up to 531 μM (SD = ±0.46, $n = 11$). These results reflected the fluctuation of FA inside the cells during the artificial intervention. More importantly, it proved that **PIPBA** could quantitatively report both spontaneous and exogenous FA in living cells.
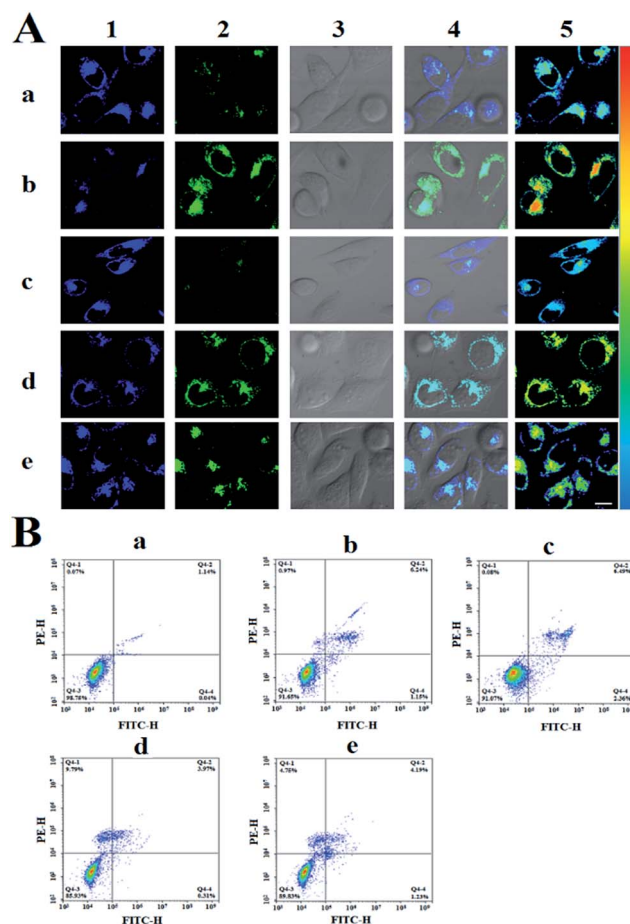

Fig. 3 Confocal imaging (A) and apoptosis assay (B) investigating the effect of intracellular formaldehyde under oxidative stress. (A) (a) HeLa cells were incubated with probe **PIPBA** (5 μM); (b) cells were incubated with formaldehyde (0.8 mM) for 2 h and then with **PIPBA** (5 μM) for 2 h; (c) cells were treated with 1 mM of 2,2-azobis[2-(2-imidazolin-2-yl) propane] dihydrochloride (AIPH) for 2 h and then with probe **PIPBA** (5 μM) for 2 h; (d) cells were treated successively with formaldehyde (0.8 mM) and AIPH (1 mM) for 2 h, and then **PIPBA** (5 μM) for 2 h; (e) as a contrast, cells were pretreated with HSO_3^- (0.4 mM) for 30 min, prior to the 2 h of incubation with probe **PIPBA** (5 μM), both formaldehyde (0.8 mM) and AIPH (1 mM) were then added for 2 h. Confocal imaging: green channel ($\lambda_{ex} = 405$ nm, $\lambda_{em} = 480{-}580$ nm), blue channel ($\lambda_{ex} = 405$ nm, $\lambda_{em} = 420{-}480$ nm), ratio imaging (I_{green}/I_{blue}), scale bar: 20 μm. (B) The corresponding apoptosis analysis: areas of Q4-1, Q4-2, Q4-3, and Q4-4 correspond to necrotic, late apoptosis, viable, and early apoptosis, respectively. Averages of the data were calculated, and statistical analysis was performed using the Students t-test ($n = 10$ fields of cells), **$P < 0.05$.

Investigating the mechanism of the indirect oxidative toxicity of intracellular FA

With the satisfactory optical behavior of **PIPBA**, we then set out to perform the fourth stage of intracellular experiments, aiming to explore the biological role of FA in indirect oxidative toxicity to cells. Intracellular oxidative stress could be induced by the imbalance between ROS and antioxidants. Excess ROS would cause a number of biological influences such as mutagenesis and subsequently cell apoptosis.[53–55] Inside cells, FA co-exists

with various reactive radicals that might oxidize FA to electronically excited carbonyl species or peroxyl acids.[17] These products possessed a stronger oxidizing capacity than their original forms, thus would cause enhanced damage to the cells.[56,57] In this context, we reason that the coexistence of FA with reactive radicals might induce up-regulated apoptosis or necrosis to living cells, which could account for the indirect oxidative toxicity of FA. To explore such a biological role, we incubated the HeLa cells with a radical initiator, 2,2-azobis[2-(2-imidazolin-2-yl)propane] dihydrochloride (AIPH),[58] and monitored intracellular FA and cellular state using confocal imaging and flow cytometry, respectively. First, the HeLa cells were pre-treated with probe **PIPBA** (5 μM) for 30 min as the control group. The spontaneously generated FA is indicated by the green fluorescence in Fig. 3A-a and the cellular state was estimated to be 98.75% viability + 0.07% necrosis + 1.14% late apoptosis + 0.04% early apoptosis (Fig. 3B-a). It could be seen that the low level of spontaneous FA inside the cells led to an insignificant influence on the viability of cells. Then, we incubated the control group with 0.8 mM of FA for 2 h. Due to the excess of FA, the cells exhibited enhanced fluorescence in green channel and weakened fluorescence in blue channel (Fig. 3A-b). In such a case, the late apoptosis rate was significantly increased to 6.24% (Fig. 3B-b), implying that the excessive FA had an apoptotic influence on cells. Next, we incubated intact HeLa cells with AIPH (1 mM) before the incubation with **PIPBA**, in order to induce the generation of peroxyl radicals in cells. As shown in Fig. 3A-c, the cells exhibited negligible fluorescence in the green channel, indicating that FA was consumed by the peroxyl radicals generated from AIPH. Meanwhile, the bright fluorescence in the blue channel showed that the amount of probe **PIPBA** in cells was only slightly decreased, which also indicated the extremely low level of FA in the presence of AIPH. In such a case, we found the cellular state: 91.07% viability + 0.08% necrosis + 6.49% late apoptosis + 2.36% early apoptosis (Fig. 3B-c). Comparing this with Fig. 3B-a, Fig. 3B-c showed an obvious increase in late apoptosis. This comparison reflected that addition of AIPH caused an injurious effect to normal HeLa cells by up-regulating late apoptosis. Following this result, we incubated the cells of group b with AIPH (1 mM) in order to explore the role of FA under the action of radicals. As a result, Fig. 3A-d showed enhanced fluorescence in the green channel and weakened fluorescence in the blue channel relative to Fig. 3A-c, indicating the excess of FA in presence of AIPH. Under such a condition, as could be seen from Fig. 3B-d, the cellular state was: 85.93% viability + 9.79% necrosis + 3.97% late apoptosis + 0.31% early apoptosis. Considering the above effects of individual FA and AIPH to cells, evidently, the elevated necrosis (relative to Fig. 3B-b) and the declined late apoptosis (relative to Fig. 3B-c) were not caused by the individual FA itself or AIPH-induced radicals. These results indicated that cells suffered enhanced oxidative damage that was caused by more injurious substances rather than the individual FA or AIPH-induced radicals. Considering that FA could induce the increment of high reactive oxidative species in the presence of free radical initiator, we concluded that FA contributed to the more serious indirect oxidative toxicity *via* the reaction with free

radicals. To confirm this conclusion, we used HSO_3^- (0.4 mM) as the FA scavenger to pre-treat the cells before the following incubation with FA (0.8 mM) and AIPH (1 mM). From the Fig. 3A-e, we could find a decreased amount of FA from the weakened green fluorescence and the enhanced blue fluorescence relative to Fig. 3A-d. Correspondingly, Fig. 3B-e showed a decreased necrosis rate and increased apoptosis. These results were attributed to the fact that the reduced amount of FA led to a low level of oxidative radicals produced from the reaction of FA with AIPH-induced radicals. Therefore, the FA scavenging experiments confirmed the role of FA in the mechanism of indirect oxidative toxicity, in that the reaction of FA with free radicals resulted in the more injurious substances. To further verify this conclusion, we performed cross-validation based on the confocal imaging of intracellular FA. From the ratio images in Fig. 3A, we found a smaller amount of FA in Fig. 3A-c5 than in Fig. 3A-a5, indicating that the addition of AIPH led to the decrease of endogenous FA. Together with Fig. 3B-a and c, these results confirmed the consumption of endogenous FA in cells upon addition of AIPH. Furthermore, from the comparison of Fig. 3A-b5 and d5, we found, the addition of AIPH also resulted in the decrement of FA that was exogenously added to cells. Thus, the results of cross-validation verified once again that both the endogenous and exogenous FA could be consumed by free radicals. Consequently, on the basis of the above experiments, it could be concluded that when FA exerted its indirect oxidative toxicity, it participated with the reaction in the presence of radical initiator and contributed to the generation of highly reactive oxidative species that caused more serious damage.

Imaging of FA *in vivo* in zebrafish

The above assay showed that probe **PIPBA** exhibited excellent behaviour in living cells, which inspired us to explore its application *in vivo*. Zebrafish have around 87% homologous genes with humans and have been extensively applied for fluorescent probe research.[59] Thus, we chose zebrafish as the *vivo* model to preliminarily evaluate the applicability of **PIPBA** before a following study in mammals. The zebrafish were pre-treated with 5 μM **PIPBA** for 3 h in an E3 medium. The fluorescence signal in the green channel was collected, as shown in Fig. 4a, visualizing the endogenous FA in the zebrafish. Then, to verify this finding, we pre-treated the zebrafish with 500 μM of HSO_3^- for 1 h before the following 3 h of incubation with **PIPBA** (5 μM). As a result, Fig. 4b-2 shows a negligible fluorescence signal in the green channel. This result indicated that the endogenous FA was almost exhausted by the FA scavenger HSO_3^-, and thus confirmed that the green fluorescence collected in Fig. 4a could be attributed to the endogenous FA in zebrafish. Next, for the further confirmation, the exogenous FA (1 mM; 2 mM) was added to the above zebrafish. From the results shown in Fig. 4c and d, we found an enhanced fluorescence intensity in the green channel accompanied by remarkably weakened fluorescence in the blue channel. These results manifested the fact that the overwhelming FA level exhausted the HSO_3^- in the zebrafish, re-triggering the green fluorescence,
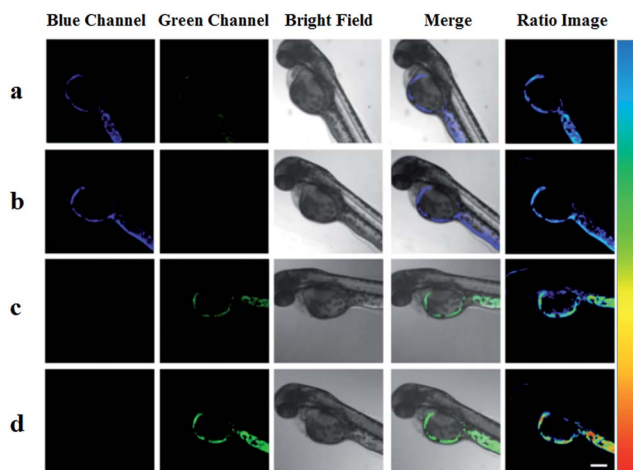
Fig. 4 Confocal imaging of endogenous formaldehyde in zebrafish. In (a) the zebrafish was treated with 5 μM PIPBA for 3 h in an E3 medium. In (b) the zebrafish was treated first with 500 μM of HSO_3^- for 1 h, and then with PIPBA (5 μM) for 3 h. In (c and d) the zebrafish of group b was treated with formaldehyde (1 mM; 2 mM) for 3 h. Fluorescence images: green channel (λ_{ex} = 405 nm, λ_{em} = 480–580 nm), blue channel (λ_{ex} = 405 nm, λ_{em} = 420–480 nm), ratio imaging (I_{green}/I_{blue}), scale bar: 200 μm.

and, correspondingly, the exhaustion of PIPBA resulted in negligible fluorescence in the blue channel. Therefore, the above experiments showed that probe PIPBA was capable of imaging FA in zebrafish, providing an important reference for the following experiments in mice.

Investigating the biological role of FA in the renal tissue of living mice

The satisfactory behaviour of PIPBA promoted us to investigate its capability to track FA in living mice. We hope to explore the mechanism of indirect oxidative toxicity of FA in the kidney tissue of living mice with the aid of PIPBA. Prior to the collection of fluorescence intensity, optimal scanning depths for PIPBA in renal tissue were investigated. As shown in Fig. S11,† the fluorescence intensity displayed heterogeneous distribution at various depths, and the highest intensity could be recorded at depths interval of 60–80 μm. Thus, confocal scanning for renal samples was performed at the depth of 80 μm to achieve intense and stable fluorescence signals in the following *in vitro* and *in vivo* experiments. According to practical conditions, we performed the experiments in three stages step by step. As the first stage, confocal imaging analysis of FA *in vitro* was performed to provide a trial as well as a validation for FA imaging in the kidney. The fresh kidney was harvested from a mouse. The slice (400 μm) was analyzed using confocal fluorescence imaging after being incubated in a medium containing PIPBA (5 μM) for 2 h. As shown in Fig. 5B-a, the green channel presented a weak intensity, implying the existence of spontaneous FA in the kidney samples. To confirm this finding, 200 μM of HSO_3^- was used to pre-treat the slices for 30 min before the incubation with PIPBA. The excessive HSO_3^- would dramatically consume the spontaneous FA, which could in turn confirm the spontaneous

FA. As expected, Fig. 5B-b exhibited negligible fluorescence intensity in the green channel and an enhanced fluorescence intensity in the blue channel, relative to those in Fig. 5B-a. These results indicated the consumption of FA by excessive HSO_3^-, and excluded the possibility that the green fluorescence collected in Fig. 5B-a was induced by other interfering compounds or background in tissue. The ratio images (Fig. 5B-a4 and b4) illustrate the difference in FA level between these two groups. In the next experiments, increasing levels of FA (250 μM; 750 μM) were used to incubate the samples from Fig. 5B-b. As a result, both Fig. 5B-c and d showed increasing fluorescence intensity in the green channel and decreasing fluorescence intensity in the blue channel. The ratio images also reflected the increasing trend of I_{green}/I_{blue}. Clearly, these results were consistent with the increasing levels of FA. Therefore, *in vitro* experiments demonstrated that PIPBA could visually report both endogenous and exogenous FA in kidney slices, which inspired us to perform the application of PIPBA *in vivo*. Thus, in the second stage, we performed the *in vivo* experiments by injecting PIPBA intraperitoneally to living mice to estimate the capability of PIPBA to track the endogenous FA *in vivo*. First, the mice were injected intraperitoneally with 500 μL of saline (0.9%). After 2 h, these mice were injected with 40 μL of probe PIPBA (25 μM) and then incubated for 2 h. The tested mice were anesthetized *via* intraperitoneal injection of chloral hydrate (4%; 3 mL kg^{-1}) and laparotomized to expose the kidney. Saline was injected to wash blood off, and a slice (400 μm) was cut from the intravital kidney for the confocal imaging assay. As displayed in Fig. 5C-a, the weak fluorescence intensity in the green channel was collected, indicating the spontaneous FA in the intravital kidney. Since BTSA (*N*-benzyl-2,4-dinitrophenylsulfonamide) could stimulate the organism to generate endogenous HSO_3^-, we thought that this compound could be used as the FA scavenger (Fig. S15 and S16†) *in vivo*. Then, we injected mice intraperitoneally with 500 μL of saline (0.9%) containing 500 μM of BTSA. We reasoned that the endogenously generated HSO_3^- would scavenge the endogenous FA in organism. After 2 h, these mice were injected with 40 μL of probe PIPBA (25 μM) and then incubated for another 2 h. As shown in Fig. 5C-b, weakened green fluorescence and enhanced blue fluorescence were observed, indicating the reduced level of FA from the action of endogenously generated HSO_3^-. These results demonstrated that probe PIPBA was capable of monitoring the fluctuation of FA *in vivo*, which encouraged us to explore the histopathology of an FA-damaged kidney, in order to explore the indirect oxidative toxicity of FA in living tissue. The contextual information about such an exploration lay in the fact that FA has been found to show toxicity to the urinary system,[60] leading to glomerular degeneration and tubular congestion.[61] In this context, we set out to perform the third stage of the experiment to monitor the FA-damaged renal tissue that was protected by antioxidants. First, mice were injected intraperitoneally with saline (0.9%) every other day for 2 weeks as the control. The tested mice were intraperitoneally injected with PIPBA (25 μM). After 2 h, the mice were anesthetized using an intraperitoneal injection of chloral hydrate (4%; 3 mL kg^{-1}) and vivisected to expose the kidney. The slices
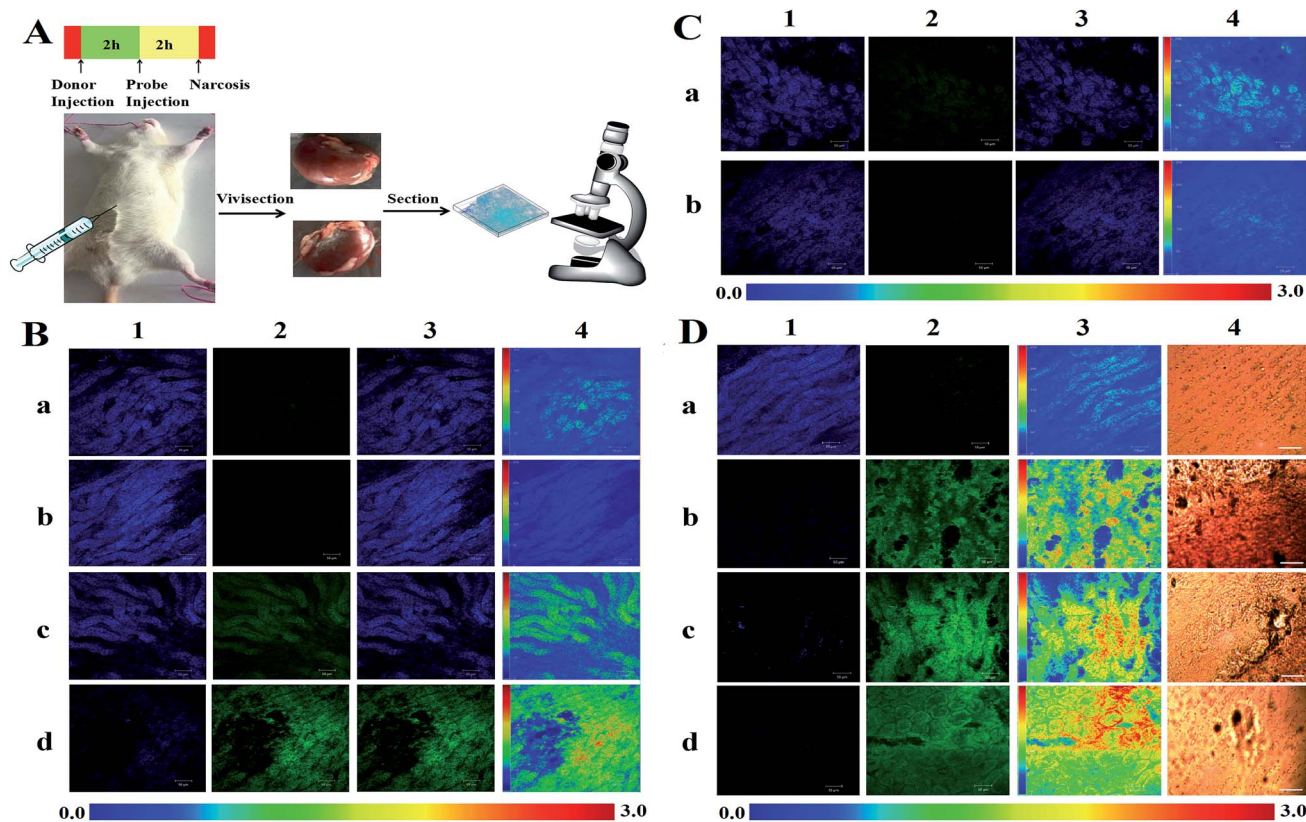
Fig. 5 (A) The schematic depiction of confocal imaging of formaldehyde in the renal tissue of living mice. (B) Confocal imaging of kidney tissue slices (400 μm) pre-treated with: (a) **PIPBA** (5 μM) for 2 h; (b) 200 μM HSO_3^- for 30 min and then **PIPBA** (5 μM) for 2 h; (c) **PIPBA** (5 μM) for 30 min and then formaldehyde (250 μM) for 2 h; (d) **PIPBA** (5 μM) for 30 min and then formaldehyde (750 μM) for 2 h. (C) Confocal imaging of endogenous formaldehyde in kidney slices of living mice. (a) Mice were injected with saline (0.9%), and after 2 h, mice were intraperitoneally injected with saline (0.9%) containing probe **PIPBA** (25 μM) for another 2 h; (b) mice were intraperitoneally injected successively with saline (0.9%) containing BTSA (500 μM) and after 2 h were injected with the saline (0.9%) containing probe **PIPBA** (25 μM). After 2 h, the mice were anesthetized *via* intraperitoneal injection of chloral hydrate (4%; 3 mL kg^{-1}) and vivisected to expose the kidney. Saline (0.9%) was injected to wash blood off and slices (400 μm) were cut from the kidney for the confocal imaging. (D) Confocal imaging of formaldehyde in the kidney slices from the mice: (a) mice were injected intraperitoneally with saline (0.9%) every other day for 2 weeks; (b) mice were intraperitoneally with FA (10 mg kg^{-1}) diluted by saline every other day for 2 weeks; (c and d) mice were intraperitoneally injected with FA (10 mg kg^{-1}) and vitamin E (20 mg kg^{-1} (c), 40 mg kg^{-1} (d)), respectively and alternately every other day for 2 weeks. The mice were anesthetized *via* intraperitoneal injection of chloral hydrate (4%; 3 mL kg^{-1}) and vivisected to expose the kidney. Saline (0.9%) was injected to wash blood off and slices (400 μm) were cut from the kidney for confocal imaging. Fluorescence images: green channel ($\lambda_{ex} = 405$ nm, $\lambda_{em} = 480–580$ nm), blue channel ($\lambda_{ex} = 405$ nm, $\lambda_{em} = 420–480$ nm), ratio imaging (I_{green}/I_{blue}), scale bar: 50 μm. All animal experiments were performed in full compliance with international ethical guidelines. List 1 and list 2 were, respectively, the blue and green channels; for B and C, list 3 and 4 were respectively the merged images (list 1 + list 2) and ratio images; for D, list 3 and 4 were respectively the ratio images and the morphological study of renal histology using a polarizing microscope.

were cut from the kidney and then analysed *via* fluorescence confocal imaging. In Fig. 5D-a, the ratio images showed that FA in control group was at the low concentration level. Meanwhile the renal tissue was orderly and smooth (Fig. 5D-a4), indicating the healthy state of the kidney in control groups. Then, FA-induced renal damage was caused to healthy mice by intraperitoneally injecting the mice with FA (10 mg kg^{-1}, diluted by saline) every other day for 2 weeks. The slices of kidney were analyzed as illustrated in Fig. 5D-b. Remarkably, a bright green channel and weak blue channel were observed, indicating the excessive FA in the kidney of the mice. Meanwhile, in this group, the damaged renal tissue showed severe degenerative changes and shrinkage of cytoplasm, as well as the loss of integrity and epithelial glossiness (Fig. 5D-b4).[62,63] To

implement protection against the toxicity of FA, we selected a well-known radical scavenger vitamin E to remove the free radicals.[64] Mice were intraperitoneally injected with FA (10 mg kg^{-1}) and vitamin E (20 mg kg^{-1}; 40 mg kg^{-1}) respectively and alternately every other day for 2 weeks. From results shown in Fig. 5D-c4, we found less tissue damage and decreased generation of epithelial cells with higher flatness. Moreover, Fig. 5D-d4 shows an enhanced protective effect upon the addition of more vitamin E. It is worth noting that, the confocal imaging showed increased amounts of FA in group c and d relative to group b in Fig. 5D. These findings indicated that FA was not consumed by the added vitamin E, though vitamin E exerted its protective effect against FA. In fact, as shown in Fig. 5D-c3 and d3, FA was slightly increased in some regions. Since vitamin E

and FA are both reductants, we supposed that vitamin E consumed reactive oxidative species in the organism, thereby leaving more of the other reductant, FA,[17,61] which should be responsible for the increment of FA in Fig. 5D-c3 and d3. In such a case, though FA was remaining, there was not a sufficient chance for FA to fully exert its indirect oxidative damage to the organism by reacting with free radicals in the presence of the effective antioxidant vitamin E. In return, this result supported the indirect oxidative toxicological mechanism that FA could react with reactive oxidative species to produce more oxidizing free radicals eventuating in oxidative damage to organism, which was consistent with the investigation of intracellular FA under oxidative stress in the present work. Therefore, the above experiments demonstrated that **PIPBA** is an outstanding probe for in-depth exploration of FA in physiological and pathological processes.

Conclusions

In summary, we have constructed a new bright, sensitive ratiometric fluorescent probe **PIPBA** for FA imaging and mechanistic exploration. The π-extended modification of phenylphenanthroimidazole provided the fluorophore featuring bright and stable fluorescence emission. The transformable intramolecular charge transfer (ICT) in **PIPBA** allowed this probe a large red shift in emission wavelength when sensing FA. Probe **PIPBA** was endowed with outstanding properties including high quantum yields, a sensitive ratiometric response and a low detection limit. For the first time, intracellular quantification and *in vivo* imaging, as well as living tissue imaging of endogenous FA that was spontaneously generated by a living organism, were enabled. Furthermore, the exploration of the biological role of FA in indirect oxidative damage to living cells and renal tissue in living mice were realized using fluorescence imaging. It was found that, despite being a reductant, FA exerted indirect oxidative damage by participating in reactions with free radicals, and thus caused enhanced damage to living organisms. This work presented a breakthrough in FA imaging and exploration in living systems. We therefore anticipate that **PIPBA** may be employed as a powerful tool to perform further studies of FA in living organisms.

Live subject statements

Zebrafish and Kunming mice were purchased from Changzhou Cavens Lab Animal Co. Ltd. All experimental procedures were conducted in conformity with institutional guidelines for the care and use of laboratory animals, and protocols were approved by the Institutional Animal Care and Use Committee in Binzhou Medical University, Yantai, China. Approval number: no. BZ2014-102R.

Conflicts of interest

There are no conflicts to declare.

Acknowledgements

Notes and references

1 L. E. Heim, N. E. Schlörer, J.-H. Choi and M. H. Prechtl, *Nat. Commun.*, 2014, **5**, 3621–3629.
2 A. Moghaddam, W. Olszewska, B. Wang, J. S. Tregoning, R. Helson, Q. J. Sattentau and P. J. Openshaw, *Nat. Med.*, 2006, **12**, 905–907.
3 J. L. Costa and D. L. Murphy, *Nature*, 1975, **255**, 407–408.
4 T. Salthammer, S. Mentese and R. Marutzky, *Chem. Rev.*, 2010, **110**, 2536–2572.
5 N. H. Chen, K. Y. Djoko, F. J. Veyrier and A. G. Mcewan, *Front. Microbiol.*, 2016, **7**, 257–274.
6 S. C. Trewick, T. F. Henshaw, R. P. Hausinger, T. Lindahl and B. Sedgwick, *Nature*, 2002, **419**, 174–178.
7 Y. Lai, R. Yu, H. J. Hartwell, B. C. Moeller, W. M. Bodnar and J. A. Swenberg, *Cancer Res.*, 2016, **76**, 2652–2661.
8 K. J. Denby, J. Iwig, C. Bisson, J. Westwood, M. D. Rolfe, S. E. Sedelnikova, K. Higgins, M. J. Maroney, P. J. Baker and P. T. Chivers, *Sci. Rep.*, 2016, **6**, 38879–38886.
9 M. Hauptmann, P. A. Stewart, J. H. Lubin, L. E. B. Freeman, R. W. Hornung, R. F. Herrick, R. N. Hoover, J. F. Fraumeni, A. Blair and R. B. Hayes, *J. Natl. Cancer Inst.*, 2009, **101**, 1696–1708.
10 K. Tulpule and R. Dringen, *J. Neurochem.*, 2013, **127**, 7–21.
11 I. Zararsiz, M. F. Sonmez, H. R. Yilmaz, U. Tas, I. Kus, A. Kavakli and M. Sarsilmaz, *Toxicol. Ind. Health*, 2006, **22**, 223–229.
12 R. C. Grafstrom, R. D. Curren, L. L. Yang and C. C. Harris, *Science*, 1985, **228**, 89–91.
13 R. Yu, Y. Lai, H. J. Hartwell, B. C. Moeller, M. Doyle-Eisele, D. Kracko, W. M. Bodnar, T. B. Starr and J. A. Swenberg, *Toxicol. Sci.*, 2015, **146**, 170–182.
14 S. Karmakar, E. M. Harcourt, D. S. Hewings, F. Scherer, A. F. Lovejoy, D. M. Kurtz, T. Ehrenschwender, L. J. Barandun, C. Roost and A. A. Alizadeh, *Nat. Chem.*, 2015, **7**, 752–758.
15 S. K. Archer, N. E. Shirokikh, T. H. Beilharz and T. Preiss, *Nature*, 2016, **535**, 570–574.
16 J. M. Thomas, R. Raja, G. Sankar and R. G. Bell, *Nature*, 1999, **398**, 227–230.
17 Y. Saito, K. Nishio, Y. Yoshida and E. Niki, *Toxicology*, 2005, **210**, 235–245.
18 S. Teng, K. Beard, J. Pourahmad, M. Moridani, E. Easson, R. Poon and P. J. O'Brien, *Chem.-Biol. Interact.*, 2001, **130–132**, 285.
19 E. Janos, J. Balla, E. Tyihak and R. Gaborjanyi, *J. Chromatogr. A*, 2015, **191**, 239–244.

20 P. H. Yu, C. Cauglin, K. L. Wempe and D. Gubisnehaberle, *Anal. Biochem.*, 2003, **318**, 285–290.

21 T. F. Brewer, G. Burgos-Barragan, N. Wit, K. J. Patel and C. J. Chang, *Chem. Sci.*, 2017, **8**, 4073–4081.

22 L. Yuan, L. Wang, B. K. Agrawalla, S.-J. Park, H. Zhu, B. Sivaraman, J. Peng, Q.-H. Xu and Y.-T. Chang, *J. Am. Chem. Soc.*, 2015, **137**, 5930–5938.

23 Z. Lou, P. Li and K. Han, *Acc. Chem. Res.*, 2015, **48**, 1358–1368.

24 C. R. Suri, R. Boro, Y. Nangia, S. Gandhi, P. Sharma, N. Wangoo, K. Rajesh and G. S. Shekhawat, *TrAC, Trends Anal. Chem.*, 2009, **28**, 29–39.

25 M. Gao, F. Yu, C. Lv, J. Choo and L. Chen, *Chem. Soc. Rev.*, 2017, **46**, 2237–2271.

26 X. Chen, F. Wang, J. Y. Hyun, T. Wei, J. Qiang, X. Ren, I. Shin and J. Yoon, *Chem. Soc. Rev.*, 2016, **45**, 2976–3016.

27 H. Chen, Y. Tang and W. Lin, *TrAC, Trends Anal. Chem.*, 2016, **76**, 166–181.

28 Y. H. Lee, Y. Tang, P. Verwilst, W. Lin and J. S. Kim, *Chem. Commun.*, 2016, **52**, 11247–11250.

29 T. F. Brewer and C. J. Chang, *J. Am. Chem. Soc.*, 2015, **137**, 10886–10889.

30 K. J. Bruemmer, R. R. Walvoord, T. F. Brewer, G. Burgos-Barragan, N. Wit, L. B. Pontel, K. J. Patel and C. J. Chang, *J. Am. Chem. Soc.*, 2017, **139**, 5338–5350.

31 Y. Tang, X. Kong, Z.-R. Liu, A. Xu and W. Lin, *Anal. Chem.*, 2016, **88**, 9359–9363.

32 S. Singha, W. J. Yong, J. Bae and K. H. Ahn, *Anal. Chem.*, 2017, **89**, 3724–3731.

33 Y. Tang, X. Kong, A. Xu, B. Dong and W. Lin, *Angew. Chem., Int. Ed.*, 2016, **55**, 3356–3359.

34 Y. Chen, C. Zhu, Z. Yang, J. Chen, Y. He, Y. Jiao, W. He, L. Qiu, J. Cen and Z. Guo, *Angew. Chem.*, 2013, **52**, 1688–1691.

35 C. Liu, C. Shi, H. Li, W. Du, Z. Li, L. Wei and M. Yu, *Sens. Actuators, B*, 2015, **219**, 185–191.

36 J. B. Li, Q. Q. Wang, L. Yuan, Y. X. Wu, X. X. Hu, X. B. Zhang and W. Tan, *Analyst*, 2016, **141**, 3395–3402.

37 J. Xu, Z. Yue, L. Zeng, J. Liu, J. M. Kinsella and R. Sheng, *Talanta*, 2016, **160**, 645–652.

38 Z. Xie, J. Ge, H. Zhang, T. Bai, S. He, J. Ling, H. Sun and Q. Zhu, *Sens. Actuators, B*, 2017, **241**, 1050–1056.

39 L. He, X. Yang, Y. Liu, X. Kong and W. Lin, *Chem. Commun.*, 2016, **52**, 4029–4032.

40 C. Liu, X. Jiao, S. He, L. Zhao and X. Zeng, *Dyes Pigm.*, 2017, **138**, 23–29.

41 Z. Sun, H. Sun, H. Li, J. You and L. Xia, *Curr. Anal. Chem.*, 2014, **10**, 381–392.

42 Z. Sun, J. You, C. Song and L. Xia, *Talanta*, 2011, **85**, 1088–1099.

43 Z. Sun, J. You, L. Xia and Y. Suo, *Chromatographia*, 2009, **70**, 1055–1063.

44 X. Han, X. Song, F. Yu and L. Chen, *Adv. Funct. Mater.*, 2017, **27**, 1700769.

45 G. Chen, C. Wang, J. You, C. Song, Z. Sun, G. Li and L. Kang, *J. Liq. Chromatogr. Relat. Technol.*, 2013, **36**, 2107–2124.

46 K. Dou, Q. Fu, G. Chen, F. Yu, Y. Liu, Z. Cao, G. Li, X. Zhao, L. Xia and L. Chen, *Biomaterials*, 2017, **133**, 82–93.

47 H. Song, S. Rajendiran, N. Kim, S. K. Jeong, E. Koo, G. Park, T. D. Thangadurai and S. Yoon, *Tetrahedron Lett.*, 2012, **53**, 4913–4916.

48 Y. Liu, X. Yang, L. Liu, H. Wang and S. Bi, *Dalton Trans.*, 2015, **44**, 5354–5363.

49 Y. Liu, G. Chen, H. Wang, S. Bi and D. Zhang, *Eur. J. Inorg. Chem.*, 2014, **2014**, 2502–2511.

50 L. Liu, Y. Liu, B. Ling and S. Bi, *J. Organomet. Chem.*, 2017, **827**, 56–66.

51 Y. Liu, Y. Tang, Y.-Y. Jiang, X. Zhang, P. Li and S. Bi, *ACS Catal.*, 2017, **7**, 1886–1896.

52 Y. Ding, J. Li, J. R. Enterina, Y. Shen, I. Zhang, P. H. Tewson, G. C. H. Mo, J. Zhang, A. M. Quinn, T. E. Hughes, D. Maysinger, S. C. Alford, Y. Zhang and R. E. Campbell, *Nat. Methods*, 2015, **12**, 195–198.

53 D. Trachootham, J. Alexandre and P. Huang, *Nat. Rev. Drug Discovery*, 2009, **8**, 579–591.

54 L. Muinelo-Romay, L. Alonso-Alconada, M. Alonso-Nocelo, J. Barbazan and M. Abal, *Curr. Mol. Med.*, 2012, **12**, 746–762.

55 C. Gorrini, I. S. Harris and T. W. Mak, *Nat. Rev. Drug Discovery*, 2013, **12**, 931–947.

56 W. Adam, A. Kurz and C. R. Saha-Möller, *Free Radical Biol. Med.*, 1999, **26**, 566–579.

57 R. J. Carmody and T. G. Cotter, *Redox Rep.*, 2001, **6**, 77–90.

58 K. Terao and E. Niki, *J. Free Radicals Biol. Med.*, 1986, **2**, 193–201.

59 Y. Liu, D. Li and Z. Yuan, *Appl. Sci.*, 2016, **6**, 392–399.

60 M. J. Sarnak, J. Long and A. J. King, *Clin. Nephrol.*, 1999, **51**, 122–125.

61 I. Zararsiz, M. F. Sonmez, H. R. Yilmaz, U. Tas, I. Kus, A. Kavakli and M. Sarsilmaz, *Toxicol. Ind. Health*, 2006, **22**, 223–229.

62 M. Gulec, A. Gurel and F. Armutcu, *Mol. Cell. Biochem.*, 2006, **290**, 61–67.

63 A. Gurel, O. Coskun, F. Armutcu, M. Kanter and O. A. Ozen, *J. Chem. Neuroanat.*, 2005, **29**, 173–178.

64 P. Poprac, K. Jomova, M. Simunkova, V. Kollar, C. J. Rhodes and M. Valko, *Trends Pharmacol. Sci.*, 2017, **38**, 592–607.